Accepted Manuscript

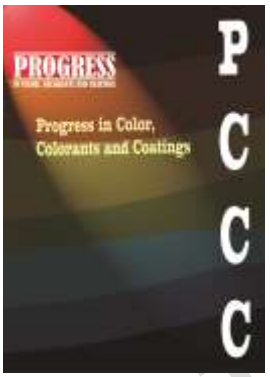

Title: Corrosion Inhibition of Mild Steel in 1 M HCl Using 5-(3-Methylphenyl)-4-((4-Nitrobenzylidene)amino)-4H-1,2,4-Triazole-3-Thiol: Experimental and Theoretical Insights

Authors: Z.A. Betti, H.H. Al-Doori, A.F. Mahmood, A.A. Alamiery

Manuscript number**: PCCC-2502-1359**

To appear in: Progresss in Color, Colorants and Coatings

Received: 2 February 2025

Final Revised: 12 May 2025

Accepted: 18 May 2025

Please cite this article as:

Z.A. Betti, H.H. Al-Doori, A.F. Mahmood, A.A. Alamiery, Corrosion Inhibition of Mild Steel in 1 M HCl Using 5-(3-Methylphenyl)-4-((4-Nitrobenzylidene)amino)-4H-1,2,4-Triazole-3-Thiol: Experimental and Theoretical Insights, Prog. Color, Colorants, Coat., 18 (2025) XX-XXX.

DOI: 10.30509/pccc.2025.167462.1359

Corrosion Inhibition of Mild Steel in 1 M HCl Using 5-(3-Methylphenyl)-4-((4-Nitrobenzylidene)amino)-4H-1,2,4-Triazole-3-Thiol: Experimental and Theoretical Insights

Z.A. Betti [1], H.H. Al-Doori [2], A.F. Mahmood [3], A.A.Alamiery[4]

[1] Technical Engineering College, Middle Technical University, P.O. Box: 10001, Baghdad, Iraq

[2] Al-Karkh University of Science, Baghdad P.O. Box: 10001, Baghdad, Iraq

[3] Oil and Gas Engineering Department, University of Technology, Baghdad P.O. Box: 10001, Baghdad, Iraq

[4] Al-Ayen Scientific Research Center, Al-Ayen Iraqi University, AUIQ, An Nasiriyah, P.O. Box: 64004, Thi Qar, Iraq

Abstract

This study investigates the corrosion inhibition performance of 5-(3-methylphenyl)-4-((4-nitrobenzylidene)amino)-4H-1,2,4-triazole-3-thiol (MNATT) for mild steel in 1 M HCl, using both experimental weight loss techniques and Density Functional Theory (DFT) calculations. Weight loss experiments were conducted at MNATT concentrations ranging from 0.1 to 1.0 mM and immersion times between 1 and 48 hours. The highest inhibition efficiency of 88.6% was observed at 0.5 mM after 5 hours of immersion. A temperature-dependent study conducted at 303-333 K revealed a mild improvement in inhibition performance with rising temperature, indicating thermal stability of the adsorbed layer. Adsorption behavior followed the Langmuir isotherm, and the calculated standard free energy of adsorption (ΔG^{o}_{ads} = –14.33 kJ·mol^{-1}) confirmed that the adsorption

mechanism is physisorption. Complementary DFT analysis showed a HOMO-LUMO energy gap (ΔE = 3.532 eV) and identified electron-rich active sites, supporting the molecule's ability to interact with the metal surface. These findings demonstrate that MNATT is a promising, low-concentration, surface-friendly corrosion inhibitor for mild steel in acidic environments.

Keywords: Corrosion, Mild steel, HCl, DFT, Energy gap.

1. Introduction

Mild steel is one of the most widely utilized materials in various industrial sectors due to its excellent mechanical properties, ease of fabrication, and cost-effectiveness. However, its application is significantly challenged by its high susceptibility to corrosion, particularly in acidic media such as those encountered during cleaning, pickling, acidizing of oil wells, and industrial processing [1, 2]. Corrosion not only degrades the physical integrity of steel structures but also leads to considerable economic losses and safety hazards, reinforcing the importance of developing effective corrosion mitigation strategies [3, 4]. Among the numerous approaches available, the use of organic corrosion inhibitors has been widely adopted due to their ability to adsorb onto metal surfaces, forming protective films that impede corrosive agents [5, 6]. These inhibitors typically contain heteroatoms such as nitrogen, sulfur, and oxygen, which can donate lone-pair electrons to the metal surface and thus form coordinate bonds that reinforce surface protection [7]. Within this category, triazole-based inhibitors have attracted considerable interest due to their multisite adsorption capability-a result of the three nitrogen atoms in the triazole ring. These molecules demonstrate strong affinity for metal surfaces, leading

to the formation of a stable, protective monolayer [8]. Furthermore, triazole derivatives are often electron-rich, possess suitable π-systems for interaction with d-orbitals of metals, and are considered structurally tunable, allowing for targeted molecular design [9, 10].

In this study, we investigate the corrosion inhibition potential of 5-(3-methylphenyl)-4-((4-nitrobenzylidene)amino)-4H-1,2,4-triazole-3-thiol (MNATT) on mild steel in 1 M HCl. MNATT was selected due to its unique molecular structure, which integrates a triazole core with functional moieties such as a nitro-substituted aromatic ring and a thiol group, known to enhance both adsorption behavior and electron donation capacity. Despite the extensive study of triazole derivatives, MNATT remains underexplored in the context of corrosion inhibition, presenting a novel opportunity for investigation. The corrosion inhibition efficiency of MNATT (Figure 1) is assessed using weight loss experiments over a range of concentrations (0.1-1.0 mM), immersion periods (1-48 hours), and temperatures (303–333 K). The study also employs Langmuir adsorption isotherm modeling and evaluates thermodynamic parameters to determine the nature of adsorption. In parallel, Density Functional Theory (DFT) calculations are carried out to examine the electronic structure of MNATT-specifically HOMO-LUMO energies, molecular softness, and charge distribution-to correlate theoretical descriptors with experimental performance.

Shenoy et al. highlighted how higher temperatures can enhance adsorption for certain inhibitors, indicating thermal activation of surface interaction [11]. Berrissoul et al. linked molecular orbital energies (HOMO-LUMO gap) with adsorption tendency using DFT analysis [12]. Ouakki et al. noted stabilization in inhibition efficiency with extended

immersion, which could be explained by equilibrium adsorption-there is no clear explanation for this; refer to relevant theories [13]. Sun et al. observed dual adsorption behavior of physisorption and chemisorption of N-heterocyclic inhibitors, which contributed to enhanced corrosion protection [14]. Studies by Ghaderi et al. and Kaban et al. emphasized the role of substituents (e.g., electron-donating groups) and the need for environmentally safe corrosion inhibitors [15, 16]. Damej et al. discussed the synergistic traits of some functional groups in inhibitors that helped to stabilize adsorption and reduce adsorption time for better protection [17]. Together, the last intertwined studies have outlined the importance of molecular structures, adsorption isotherms, and environmental constituents in the modeling of new corrosion inhibitors. The statement "In spite of extensive studies on the synthesis and application of various inhibitors, MNATT remains an unexplored candidate" further calls for a deeper view of MNATT.

Thus, this work not only contributes a new molecular candidate to the field but also integrates both experimental and theoretical perspectives to provide comprehensive insight into its inhibition behavior. This study aims to:

1. Investigate the effect of MNATT concentration and immersion time on corrosion inhibition efficiency using weight loss analysis.
2. Evaluate the influence of temperature (303-333 K) on inhibition performance and extract activation parameters.
3. Analyze the adsorption mechanism of MNATT using Langmuir isotherm modeling and thermodynamic calculations.
4. Employ DFT calculations to assess molecular properties (HOMO, LUMO, ΔE, ΔN) and link them to observed inhibition behavior.

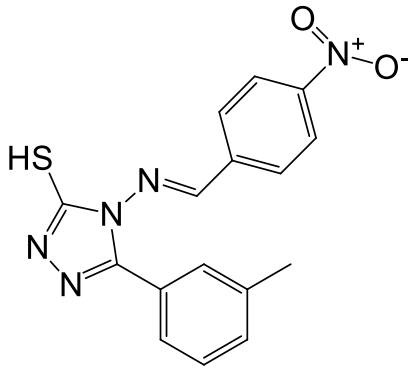

Figure 1. MNATT molecular structure

2. Experimental

Steel specimens with a composition of 0.21 % carbon, 0.05 % sulfur, 0.05 % manganese, 0.38 % silicon, 0.09 % phosphorus, 0.01 % aluminum, and the rest iron were utilized in this investigation. Each specimen was machined to dimensions of 3×2×0.2 cm. The steel surfaces were progressively polished using silicon carbide abrasive papers of increasing grit sizes to achieve a smooth finish. After polishing, the specimens were rinsed with distilled water and acetone. This preparation was performed regarding ASTM G1-03 standards for cleaning and preparing and also evaluate coupons of corrosion test [18]. A 1 M of tested solution was prepared through dilution HCl 37% with water (bi-distilled). The corrosion inhibitor (MNATT was purchased from Sigma Aldrich Malaysia), was dissolved in the acidic solution to obtain concentrations of 0.1, 0.2, 0.3, 0.4, 0.5, and 1.0 mM for the corrosive inhibitive study.

2.1. Weight loss experiments

Measurements of mass lost were conducted to assess behavior of tested coupons in 1 M HCl and the inhibitive performance of MNATT. Pre-weighed coupons were in 100 mL of the test solutions were fully immersed (5, 10, 24, and 48 hours) at specified MNATT

concentrations. The tests were also conducted at varied temperature of 303, 313, 323, and 333 K, with 5 hours as exposure time. Post immersion, specimens were withdrawn, treated with light brushing to shun covering corrosion products as per ASTM G1-03 recommendation, washed with bi-distilled water, dried, and weighed afresh [18, 19]. Each weight loss experiment was performed in triplicate, and average values were reported with deviations within ±2%. By applying the equations 1 and 2 given below:

$$C_R = \frac{\Delta m}{A \times t} \quad (1)$$

$$\text{IE\%} = \frac{C_{R0} - C_R}{C_{R0}} \times 100 \quad (2)$$

Where Δm represents mass loss (g), A refer to aria of studied surface (m^2), and t is exposure periods (h).

2.2. DFT

DFT were conducted to gain insight into electron properties of MNATT contributing to its anticorrosive mechanism. The molecular geometry of MNATT was established with the help of the function named B3LYP with 6-31G^{++} (d, p) basis set [20]. Using Koopmans's theorem [21], HOMO and LUMO of the optimized geometry were determined, from which the electron affinity (A) ionization potential (I) were evaluated (Equations 3-7). Information about the tendency of molecules to either donate or accept electrons and its relevance for interactions with metallic surfaces is indicated by these orbital energies [22].

$$E_{HOMO} = -I \quad (3)$$

$$E_{LUMO} = -A \quad (4)$$

$$\chi = (I + A) / 2 \quad (5)$$

$$\eta = (I - A) / 2 \quad (6)$$

$$\sigma = 1 / \eta \quad (7)$$

To assess transfer interaction charges between MNATT and metallic surface, The ΔN was evaluated employee formula 8:

$$\Delta N = (\chi_{Fe} - \chi_{inhibitor}) / (2 * (\eta_{Fe} + \eta_{inhibitor})) \quad (8)$$

In these calculations, the absolute hardness (η) of bulk iron is considered to be zero, and its absolute electronegativity (χ) is taken as 7.0 eV [23].

The flowchart presented in Figure 2 outlines the structured methodology employed in this study to evaluate the corrosion inhibition performance of MNATT for mild steel in 1 M HCl. The process begins with the preparation of mild steel specimens and continues with weight loss experiments conducted under varying concentrations, immersion durations, and temperatures. Based on the recorded mass loss, the inhibition efficiency is calculated and assessed under diverse experimental conditions. The experimental results are then used to interpret the adsorption behavior of MNATT, specifically through Langmuir isotherm modeling, which assumes monolayer adsorption on the metal surface. From this, thermodynamic parameters such as standard free energy of adsorption are estimated to determine whether the adsorption process is physical or chemical in nature. In parallel, DFT (Density Functional Theory) calculations are performed to obtain key electronic descriptors of the MNATT molecule, including HOMO-LUMO energy levels, molecular softness, and electrostatic potential distribution. These theoretical insights are used to identify active sites and predict adsorption affinity. The findings from both the experimental and computational approaches are finally integrated to provide a

comprehensive interpretation of MNATT's inhibitory mechanism and to correlate the electronic structure of the molecule with its observed corrosion protection performance.

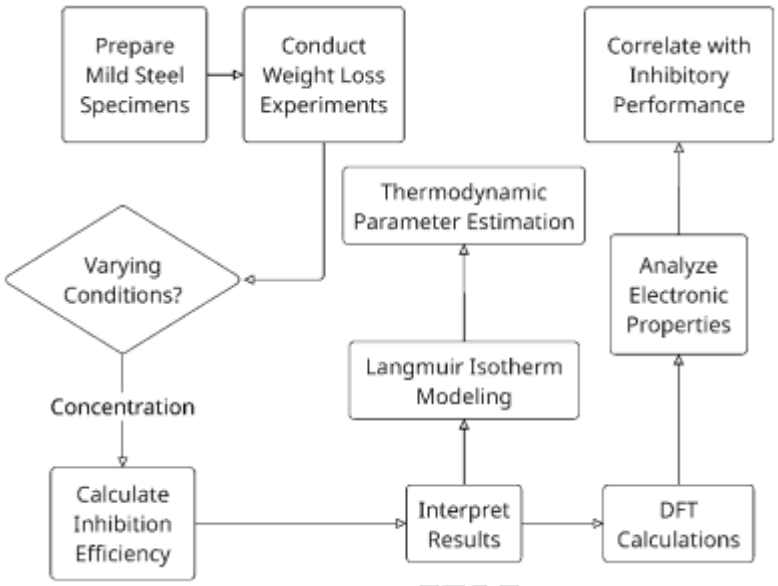

Figure 2. Workflow of the Experimental and Theoretical Methodology for Corrosion Inhibition Assessment of MNATT

3. Results and Discussion

3.1. Influence of MNATT concentration on C_R and IE

Herein, we investigates the impact of varying concentrations MNATT on the C_R and IE% of metal in HCl at 303 K. The data, as illustrated in Figure 3, demonstrate a clear relationship between MNATT concentration and its inhibitory performance.

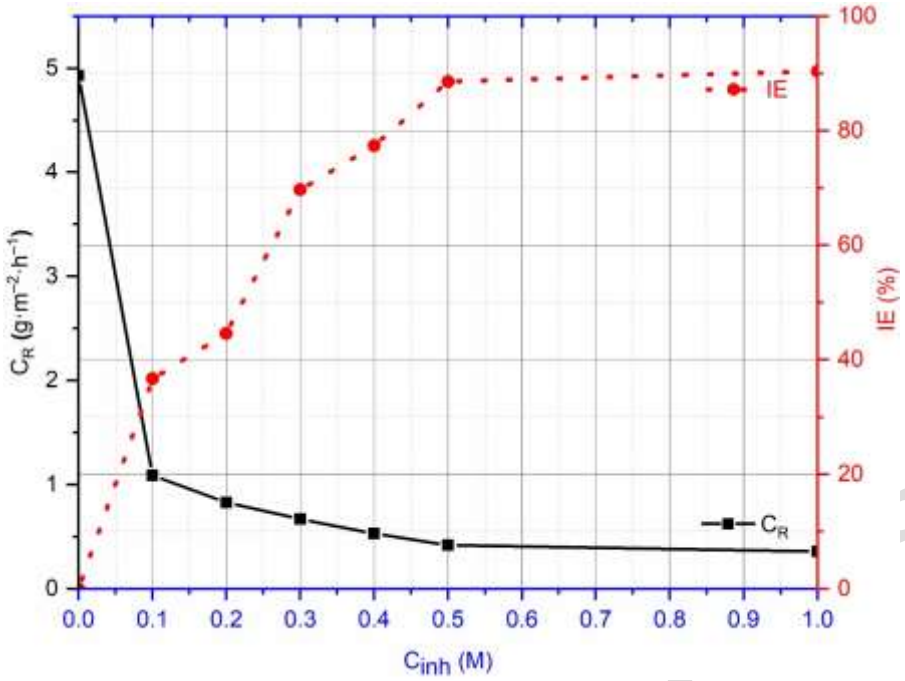

Figure 3: Impact of MNATT concentration on C_R and IE% of mild steel.

The data indicate a significant reduce in C_R with increasing MNATT concentration, followed by a an increases in inhibitive performance. At 0.1 mM MNATT, the IE is 36.7%, which increases to 88.6% at 0.5 mM. A further increase to 1.0 mM results in a marginal rise in efficiency to 90.4%, suggesting that the optimal concentration for MNATT is around 0.5 mM. MNATT mechanism is primarily due to its adsorption, forming a protective barrier that impedes corrosive attack. The heteroatoms and π-electrons in the triazole structure enhance adsorption affinity through donor-acceptor interactions with the vacant d-orbitals of iron atoms. The adsorption behavior of MNATT can be analyzed using adsorption models, that demonstrates the nature of the MNATT and the metal surface interactions [24].

In this context, to further evaluate the adsorption behavior of MNATT on mild steel in 1 M HCl, multiple adsorption isotherm models were tested, including Langmuir, Temkin, and Freundlich models. Among these, the Langmuir adsorption isotherm provided the

best linear correlation with the experimental data, as evidenced by the highest regression coefficient (R^2 = 0.9669). This indicates that the adsorption of MNATT follows a monolayer adsorption mechanism on a homogeneous metal surface with no interaction between adsorbed species. In contrast, the Temkin and Freundlich models exhibited significantly lower R^2 values, suggesting that they do not describe the system as accurately. The relatively poor fit of these models indicates that adsorption does not occur on heterogeneous sites and lateral interactions between inhibitor molecules are minimal. Therefore, the Langmuir isotherm model was selected as the most appropriate to describe the adsorption behavior of MNATT, further confirming that physisorption is the dominant mechanism under the studied conditions. Langmuir isotherm is represented by the equation 9:

$$\frac{C}{\theta} = \frac{1}{K} + C \tag{9}$$

Where C is the MNATT concentration, Θ represents surface coverage (which can be approximated by IE%/100), and K is constant of equilibrium.

A straight-line yield from plot C/Θ against C, if the adsorption follows Langmuir model, with the slope value equal one. Also 1/K and intercept have the same value. Figure 4 illustrates the Langmuir adsorption isotherm plot for the adsorption of MNATT on mild steel in 1 M HCl at 303 K. The linear relationship obtained between C_{inh}/θ and C_{inh}, with a high correlation coefficient (R^2 = 0.9669), indicates that the adsorption of MNATT follows the Langmuir adsorption isotherm model [25]. This suggests that MNATT forms a monolayer on mild steel surface, with uniform adsorption sites and no significant interactions between adsorbed molecules.

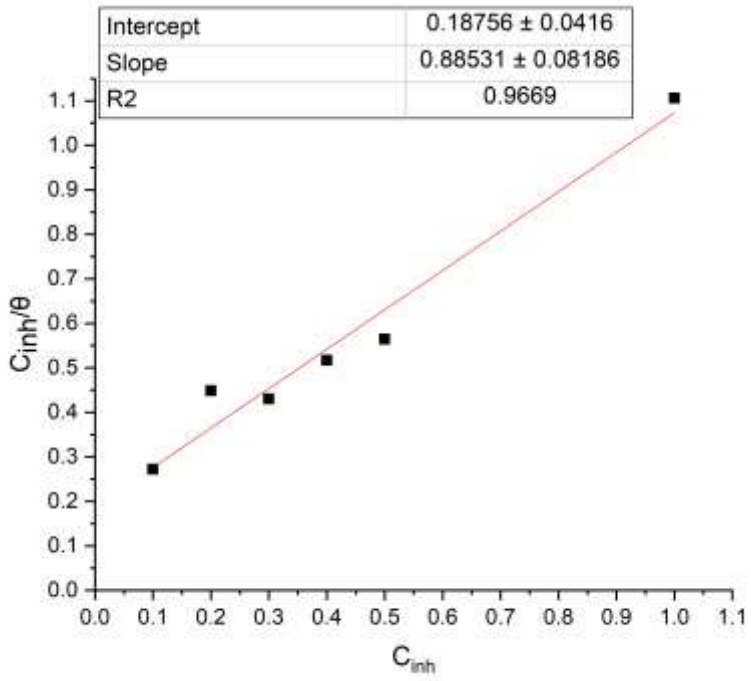

Figure 4: Plot of Langmuir Isotherm for MNATT Adsorption.

Constant of adsorption equilibrium K can be determined from the intercept. A higher K value indicates stronger adsorption affinity of MNATT molecules towards metallic surface. ΔG_{ads}^{o} was evaluated employee Eq. 10:

$$\Delta G_{ads}^{o} = -RT \ln(55.5K) \quad (10)$$

where R is constant of gas, T refere to the temperatures in Kelvin, and 55.5 represents water molar concentration.

The calculated ΔG_{ads}^{o} value provides insight into nature adsorption process. ΔG_{ads}^{o} values up to -20 kJ·mol^{-1} are consistent with physisorption, involving electrostatically interactions between inhibitor molecules and the substrate. Values more negative than -40 kJ·mol^{-1} indicate chemisorption, involving transfer between the inhibitor molecules and the substrate to form a coordinate type of bond [26-28]. In this study, the calculated ΔG_{ads}^{o} value suggests that the adsorption of MNATT on the mild steel surface occurs.

The calculated ΔG_{ads} is -14.33 kJ·mol^{-1}. This negative value indicates that the adsorption process is spontaneous. Since the magnitude is less than -20 kJ·mol^{-1}, it suggests that the adsorption mechanism follows physisorption, where the MNATT interacts with metal surface primarily through electrostatic forces rather than chemical bonding.

The adherence of MNATT to the Langmuir model implies that:

1. Single-layer adsorption occurs, meaning that once a molecule is adsorbed, no further adsorption takes place at that site.
2. No interaction exists between adjacent adsorbed molecules, suggesting that the adsorption process is independent of lateral interactions.
3. The adsorption is homogeneous, meaning all active sites on the steel surface exhibit equal affinity for MNATT molecules.

3.2. Influence of inhibitor concentration and immersion periods on corrosion rate and efficiency at 303 K

Figure 5 presents C_R and IE% of mild steel in 1 M HCl at 303 K, with different MNATT dosage and immersion times. Data elucidate the effect of both MNATT dosage and exposure duration on the protected performance of MNATT from corrosion.

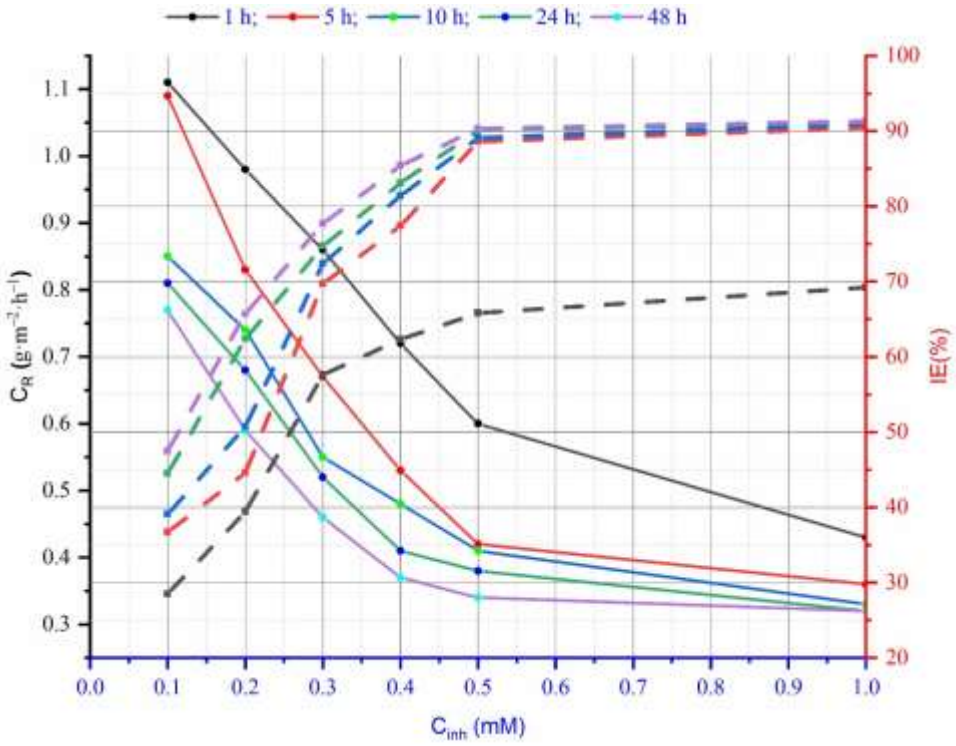

Figure 5. C_R and IE% of MNATT at 303 K

Results show that as the concentration of MNATT increases, the corrosion rate consistently declines at all immersion times. For instance, at a 1-hour immersion, the corrosion rate decreases from 1.11 g·m^{-2}·h^{-1} at 0.1 mM MNATT to 0.43 g·m^{-2}·h^{-1} at 1.0 mM. Also, the corrosion inhibition efficiency was evaluated with a 28.5-69.2% increase at the highest corrosion time; this trend prominently indicates that higher concentrations of MNATT would improve development of a stable protective film through adsorption on the metal surface, with consequent findings for a further decrease in corrosion. The effect of case exposure was found to be that increased MNATT concentration and a reduced corrosion rate are attributed to prolonged exposure; longer exposure times associated with higher inhibition. For 0.3 mM MNATT, the corrosion rate decreases from 0.86 g·m^{-2}·h^{-1} at 1 hour to 0.46 g·m^{-2}·h^{-1} at 52 hours; the inhibition efficiency varies from

57.6% to 77.7%. This suggests MNATT molecules adsorption onto surface of metal develops as time passes, culminating in more effective corrosion protection. The combined effects of MNATT concentration and immersion time flax up in a synergistic behavior of inhibition from the immersions of corrosion. At low concentrations of MNATT, i.e., 0.1 mM, the inhibition efficiency increased slowly at longer immersion times and at the end of 48 h was 47.5%. On the other hand, higher concentrations of MNATT, i.e., 1.0 mM, travelled in the range of more than 90% inhibition after just 5 h and experienced very few points of gain from the other extended period. This indicates that although extended immersion time generally enhances the inhibition efficiency of MNATT, the most effective protection can be achieved within shorter exposure periods when higher inhibitor concentrations are employed [29]. All of these trends observe the adsorption behavior of MNATT molecules on the mild steel surface. With the increase in inhibitor concentration, both sides of MNATT molecules become engulfed in corrosion on the steel surface, thus leading to corroded sites of activity and a reduction in corrosion rate. Over time, the adsorbed layer becomes compact and firm, attesting to the efficacy of that layer because of the encasement of the neutralized steel surface. The data suggest that possible saturation is being reached in the adsorption process at higher concentrations (0.5 mM and above), as indicated by very little gain (in inhibition efficiency) [30] beyond this concentration and associated immersion times. Similar studies have reported that the inhibition efficiency of organic inhibitors increases with concentration and immersion time, up to a certain point, beyond which the effect plateaus. For instance, Shukla and Ebenso [31] observed that the inhibition efficiency of streptomycin on mild steel in 1 M HCl increased with inhibitor concentration but

decreased with rising temperature, suggesting physisorption as the primary mechanism. In the present study, the sustained increase in IE with both concentration and immersion period, without a significant decrease at prolonged exposures, indicates a stable and efficient adsorption of MNATT on surface steel [32]. The comprehensive analysis of Figure 4 underscores the efficacy of MNATT as a anticorrosion compound for steel in HCl. Both increased concentration and prolonged immersion time contribute to enhanced corrosion protection, with higher concentrations.

3.3. Temperature-dependent corrosion inhibition efficiency of MNATT for mild steel in 1 M HCl solution

The data presented in Figure 6 provide a comprehensive analysis of the temperature-dependent corrosion IE of MNATT for mild steel in HCl. The study examines various concentrations of MNATT (0.1 to 1.0 mM) across a temperature range from 303 to 333 K, with a constant immersion period of 5 hours.

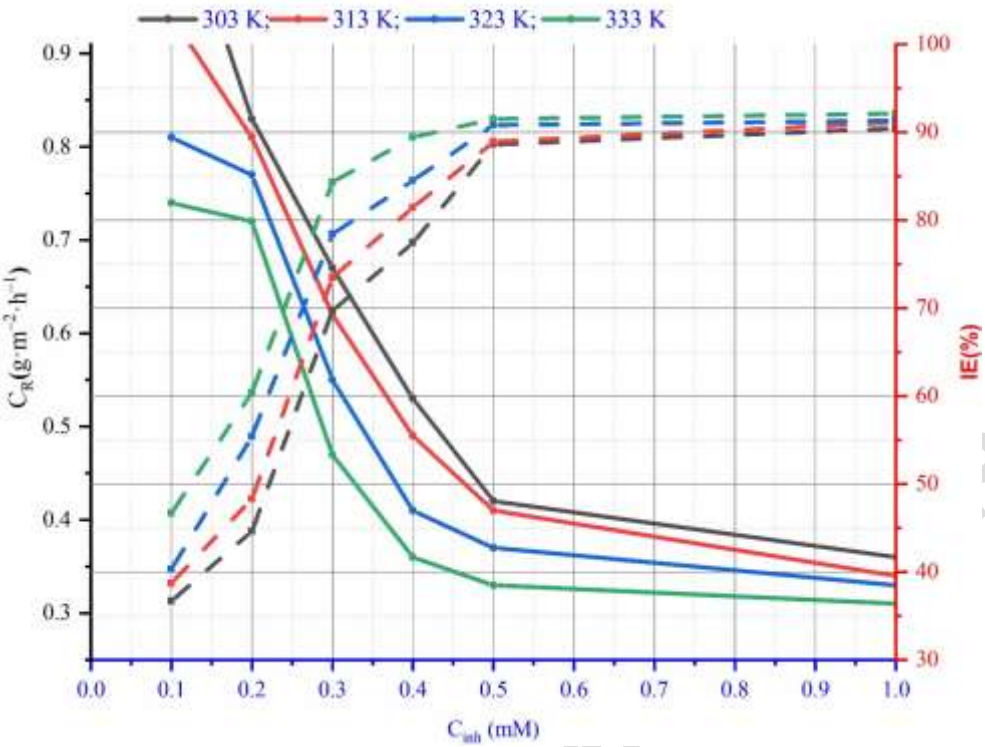

Figure 6. C_R and IE% of MNATT at different temperatures.

Data suggests a strong relationship between MNATT concentration, temperature, and rates of corrosion. C_R of mild steel was observed to decrease at higher temperatures from 303 K to 333 K with MNATT concentration being kept constant. On the opposite side, a rise in temperature has been characterized by increasing inhibition efficiency (IE%) with higher influences for the inhibition process such as temperature, time, and concentration of MNATT. Taking 0.3 mM concentration for MNATT, IE% scaled up from 69.7% at 303 K to 84.3% at 333 K. This trend signifies increased adsorption of MNATT on to the surface of mild steel sites and probably effective inhibition of this corrosive event at higher temperatures. On the other hand, IE% increases gradually with temperature but did not exceed the surrounding temperature under those of chemisorption conditions. The more the temperature increases, the better the adsorption efficiency (a heightening of the

chemisorption process) between the inhibitor molecules traversed by the metal surface; higher temperature should be supportive. Higher heat aids in the activation of the process, which, in turn, causes an increase in inhibition efficiency [33]. All the temperatures studied have, without a doubt, been accompanied by an increase in MNATT inhibition efficiency with an increase in concentration brought forth to study among 0.1 and 1.0 mM at 303 K; the increase in IE% at concentrations of 0.1 and 1.0 mM has been, respectively, 36.7, and 90.4%. For 333 K, the same behavior was observed in the inhibition efficacy jumping to a maximum for 1.0 mM with 92.1% IE. The increase in concentration of the inhibitor molecules would increase the coverage on the surface of metal, offering an effective barrier action against corrosion. Upon further evaluation of the change in IE% with temperature associated with MNATT adsorption on mild steel, it is being further implied that adsorption is an endothermic process characteristic of chemisorption. This observation of the positive impact of temperature as regards the IE% amplifies the overall support for the input that the higher temperatures would be favorable to the generation of chemical bonds between the inhibitor molecules and the metal surface; it improves the efficiency of the inhibition [34]. Here, the temperature effect on IE% implies that the adsorption process is facilitated at higher temperatures, typically evidence of chemisorptive interactions. The temperature-dependent behavior can be correlated with the behavior of some other organic inhibitors. Some research work on thiourea derivatives showed an decrease in inhibition with increasing temperature and a chemisorption mechanism. Information gathered from the summary of Figure 5 suggests that both temperature and MNATT concentration play a significant role in the corrosion inhibition efficacy for mild steel in 1 M HCl medium. To better understand the

temperature dependence of the corrosion inhibition process by MNATT, activation parameters were extracted from Arrhenius and transition state plots. These parameters include the activation energy (Ea), enthalpy of activation (ΔH), and entropy of activation (ΔS), all of which offer insight into the nature of the inhibitor-metal interaction. The Arrhenius equation (Eq. 11) was used in the form:

$$\ln C_R = \ln A - \frac{E_a}{RT} \quad (11)$$

while the transition state equation used was (Eq. 12):

$$\ln \frac{C_R}{T} = \ln \frac{k_B}{h} + \frac{\Delta S^*}{R} - \frac{\Delta H^*}{RT}$$

The resulting data as in Table 1, show that Ea decreases with increasing inhibitor concentration, indicating that MNATT effectively reduces the energy barrier for corrosion inhibition. The negative values of ΔS suggest a decrease in disorder during the formation of the activated complex, while positive ΔH values confirm the endothermic nature of the corrosion inhibition process. Figure 7 shows the Arrhenius plot for the 0.5 mM concentration, illustrating the linear relationship between ln (C_R) and 1/T. These findings are consistent with a physisorption mechanism, as indicated by the moderate Ea values and entropy trends.

Table 1: Activation Parameters from Temperature Studies

Concentration (mM)	Ea (kJ/mole)	ΔH (kJ/mole)	ΔS (kJ/mole.K)
0.1	-3.75345	-6.3973	-40.02343
0.2	-6.76031	-9.4041	-51.54909
0.3	-4.52708	-7.1709	-46.91386
0.4	-2.55429	-5.1981	-41.58424
0.5	-3.61391	-6.2577	-47.24269

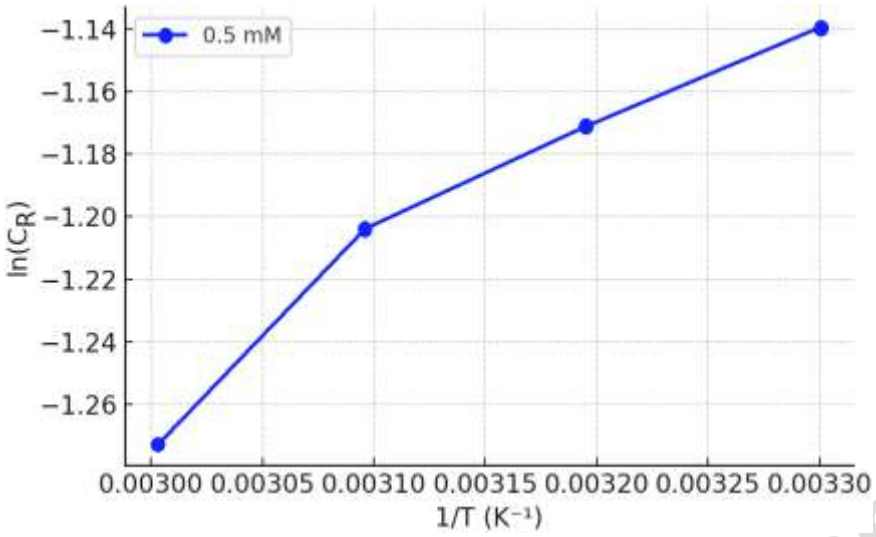

Figure 7. Arrhenius plot for the 0.5 mM.

3.4. DFT for MAPTT

Parameters evaluated based on DFT calculations are very helpful to understanding electronic properties of MNATT and efficiency as an anti-corrosion compound. Molecular orbital analysis, in this case, HOMOs and LUMOs distribution, reveal information about the reactivity and adsorption on the metal surface of the inhibitor. HOMO energy as shown in Table S1, -8.084 eV reveals that MNATT lies in being a moderate electron donor for the empty d-orbitals of Fe in mild steel. The delocalized HOMO orbitals are found around the triazole ring, sulfur, and nitrogen atoms, which indicated the vital role played by the heteroatoms in the adsorption process. The presence of nitrogen and sulfur on lone pairs supported a two-coordination to Fe atoms, hence further increasing the inhibition efficiency. Higher HOMO energy indicates a greater tendency to donate electrons to the metal surface edging toward the protective layer formation. The HOMO distribution, as appeared in the molecular structure in Figure S1, indicates that the electrons are concentrated mostly around heteroatoms, signifying better

attraction with Fe. The presence of a sulfur atom further strengthens adsorption due to soft-soft interactions with Fe atoms [35]. The LUMO energy (-4.552 eV) indicates the ability to accept electrons from the metal surface toward forming back-donation interactions. The shape of LUMO provided by the inhibitor-apparently-uses charge density from Fe, and hence further stabilizes the adsorption process. The smaller value of the LUMO energy facilitates strong back-donation from Fe. The HOMO-LUMO gap of 3.532 eV is so less, pointing to high molecular reactivity and an adsorption mechanism that is highly suitable for inhibition. Thus, the delocalization of π-electrons in the benzylidene system enhances electronic interactions with the metal surface. An energy gap of 3.532 eV between the HOMO and LUMO is a leading factor that defines the chemical reactivity of the inhibitor. A smaller HOMO-LUMO gap implies a higher electronic transition rate between the inhibitor and the metal surface, hence leading to an interactive adsorption with high inhibition efficiencies. Lower ΔE values are valuable indicators of stronger corrosion inhibition efficiency [36]. The narrow energy gap allows effective electron exchange, which stabilizes the inhibitor-metal interaction.

Electronegativity (χ = 6.318 eV) suggests that MNATT has a strong tendency to attract electrons, which helps in stabilizing adsorption. Hardness (η = 1.766 eV) is relatively low, implying that MNATT is a soft molecule, which enhances its adsorption efficiency on Fe surfaces. Softness (σ = 0.566 eV) is high, further confirming that the molecule can easily polarize and interact strongly with Fe atoms. The fraction of electrons transferred (ΔN = 0.556) indicates that MNATT donates charge to the Fe surface, confirming strong adsorption and surface interaction. Positive values of ΔN suggest spontaneous charge transfer, meaning that MNATT effectively adheres to the mild steel surface, forming a

stable protective layer.

The moderately high level of EHOMO and low level of ELUMO enable efficient electron donation and back-donation, facilitating **strong adsorption** on the metal surface. The low HOMO-LUMO gap (3.532 eV) suggests high reactivity and easy charge transfer, leading to higher inhibition efficiency. The high electronegativity and softness enhance adsorption by stabilizing the interaction with Fe atoms. The positive ΔN value confirms that charge transfer occurs from MNATT to the metal surface, ensuring strong protective layer formation. These findings strongly support the experimental inhibition efficiencies, where MNATT exhibits over 90% efficiency at optimal concentrations. The quantum chemical analysis confirms that the presence of heteroatoms (N, S), π-electron delocalization, and charge transfer properties contribute significantly to the exceptional corrosion inhibition of MNATT for mild steel in acidic environments.

Figure S2 represents the energy levels HOMO, LUMO, HOMO-1, and LUMO+1 of MNATT as determined through DFT. These energy levels provide insights into the electronic structure of the inhibitor and its efficiency in corrosion inhibition. HOMO-1 (-9.311 eV), indicating additional sites capable of donating electrons but with less reactivity compared to HOMO. HOMO (-8.084 eV), primarily responsible for electron donation to the metal surface. LUMO (-4.552 eV), which determines the electron-accepting ability from the metal surface. LUMO+1 (-1.205 eV), influencing the molecular stability and secondary electronic transitions [37]. High HOMO Energy indicates strong electron-donating ability, facilitating adsorption onto the Fe surface. The molecular structure allows lone pairs from nitrogen and sulfur to form coordination bonds with Fe, stabilizing the adsorption layer. Low LUMO Energy (-4.552 eV) suggests

efficient electron acceptance, supporting back-donation from Fe to the inhibitor molecule. The π-electron system in the benzylidene ring enhances adsorption by delocalizing electron density. Small HOMO-LUMO Energy Gap (ΔE = 3.532 eV) and a smaller gap indicates higher molecular reactivity, meaning MNATT readily donates and accepts electrons, leading to strong metal-inhibitor interactions. This enhances the surface coverage and protective film stability, directly correlating with higher inhibition efficiency. HOMO-1 (-9.311 eV) contributes additional electron-donating ability, but to a lesser extent than HOMO. LUMO+1 (-1.205 eV) suggests that MNATT has multiple electron-accepting centers, reinforcing the adsorption mechanism. The strong interaction between HOMO (electron donor) and Fe d-orbitals ensures effective surface adsorption, reducing corrosion. LUMO's ability to accept electrons from Fe stabilizes the inhibitor layer, improving efficiency. The low HOMO-LUMO gap (3.532 eV) confirms high adsorption affinity, supporting experimental findings where MNATT exhibited over 90% inhibition efficiency at optimal concentrations.

3.5. Mulliken Charges

The Mulliken atomic charge as in Figure 8, distribution provides essential information on the electron density distribution within a molecule, thereby identifying the most probable sites for nucleophilic and electrophilic interactions with the metal surface. Figure 8 displays the Mulliken charges for each atom in the MNATT molecule, as calculated through Density Functional Theory (DFT) using the B3LYP/6-31G++(d,p) basis set. The analysis reveals that atoms with higher negative charges are more likely to participate in electrostatic interactions with the positively charged metal surface, facilitating

adsorption. The nitro group (atoms O_{16} and O_{17}) shows the highest negative charges (-0.876), making it a significant contributor to electron donation and a probable site for interaction with Fe^{2+} ions. The azomethine nitrogen (N_{15}) exhibits a strong positive charge (1.119) due to polarization, potentially acting as a donor center during adsorption, particularly in coordination-type interactions. The triazole ring nitrogens (N_1, N_2, N_4) possess moderate negative charges (-0.115, -0.115, and 0.708), confirming their role in anchoring the molecule onto the metal surface. The sulfur atom (S_6), although moderately charged (0.003), still contributes due to its larger atomic radius and known affinity for iron, supporting synergistic adsorption behavior. The aromatic ring system, especially the substituted phenyl ring, contains carbon atoms with small but consistent negative charges (e.g., $C_{11} = -0.065$, $C_{12} = -0.053$), contributing to π-electron delocalization which may support physical adsorption (physisorption). The Mulliken charge distribution map confirms the multi-center adsorption ability of MNATT, where electron-rich sites such as nitrogen, oxygen, and sulfur atoms act as anchoring points during adsorption on the steel surface. This distribution supports the inhibitor's efficiency by allowing simultaneous interaction at several sites, enhancing the stability and compactness of the adsorbed inhibitor layer.

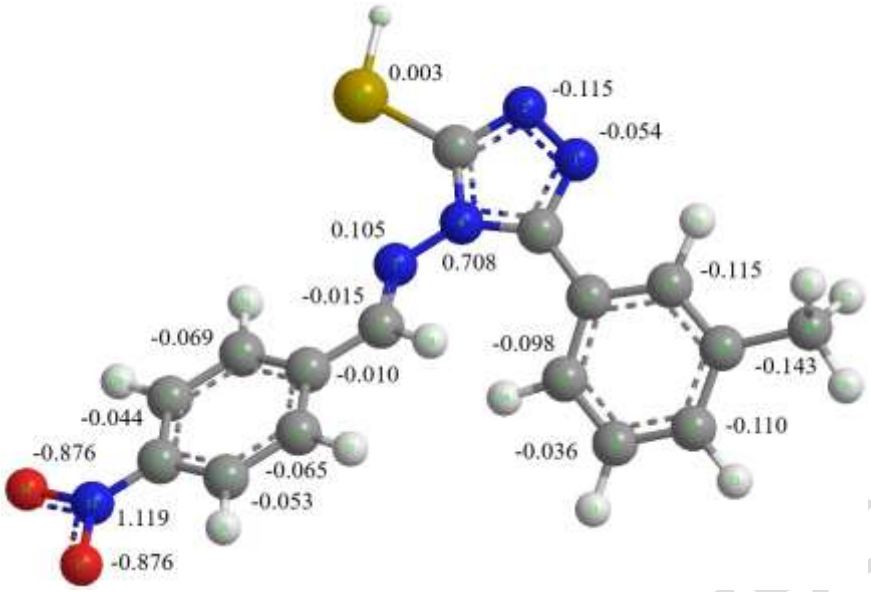

Figure 8: Mulliken Atomic Charge Distribution of MNATT Molecule Calculated Using DFT (B3LYP/6-31G++(d,p)).

3.6. Surface properties and importance of SEM analysis in corrosion studies

The surface morphology of mild steel before and after corrosion plays a crucial role in understanding the adsorption behavior of corrosion inhibitors. Scanning Electron Microscopy (SEM) is a powerful analytical technique used to examine surface modifications due to corrosion and inhibitor protection. SEM analysis provides high-resolution imaging of the steel surface at a microscopic level, allowing researchers to evaluate surface roughness and pitting formation due to corrosion, protective film formation in the presence of inhibitors and also comparative analysis of corroded and protected surfaces. The illustrative SEM-based analysis (Figure 9 a and b) conceptually depicts two key conditions of the steel surface. The 1st one when the mild steel surface after corrosion (without inhibitor) which represents the exposed to 1 M HCl, the steel undergoes severe degradation, leading to pitting, cracks, and rough surface formation. SEM analysis would typically reveal corrosion pits, increased surface roughness, and loss

of metal structure due to dissolution. The 2nd one represents the mild steel surface after corrosion (with MNATT), in the presence of MNATT, a protective layer forms on the steel surface, reducing direct acid attack and minimizing corrosion effects. SEM images in such cases usually exhibit a relatively smooth surface, with a thin adsorbed inhibitor layer, effectively shielding the steel from aggressive chloride ions.

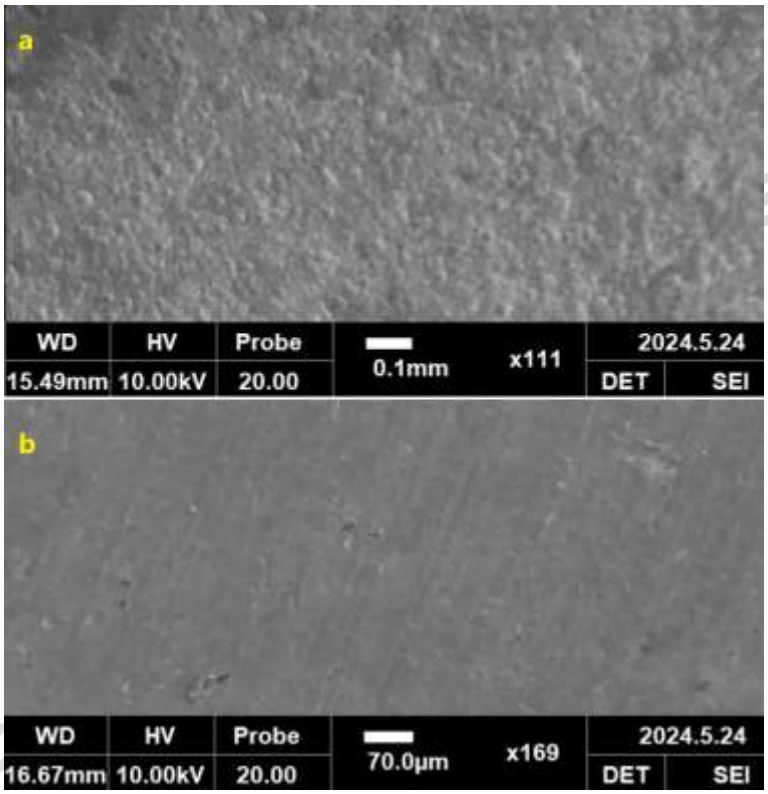

Figure 9: Conceptual illustration of SEM-based surface morphology analysis of mild steel after corrosion (a) without and (b) with MNATT Inhibitor

3.7. Suggested Inhibitive Mechanism

The mechanism of MNATT molecules as in Figure 10 follows an adsorption-based process, primarily governed by physisorption, as evidenced by the Langmuir model and the estimated standard ΔG_{ads}^{o} (-14.33 kJ·mol^{-1}). ΔG_{ads}^{o} with negative value confirms spontaneous process, but its magnitude (>-20 kJ·mol^{-1}) indicates that the interactions

between MNATT and the steel surface occurs via physisorption rather than chemical bonding. This suggests that the MNATT adhere to the substrate primarily through electrostatically interactions rather than forming covalent or coordinate bonds. Physisorption occurs when MNATT molecules interact with the (+) charged substrate via electrostatic forces. Since steel in acidic media (1 M HCl) is predominantly positively charged due to Fe dissolution ($Fe \rightarrow Fe^{2+} + 2e^{-}$), the negatively charged functional groups in MNATT, such as the nitro ($-NO_2$), triazole (-N=N-), and thiol (-SH) groups, contribute to adsorption [38]. Van der Waals forces and dipole interactions also play a role in MNATT's adhesion to the steel surface. The Langmuir isotherm model, which best fits the adsorption behavior of MNATT, suggests that:

1. The inhibitor forms a monolayer coverage over the substrate, to prevents direct contact between substrate corrosive species (Cl^- and H^+ ions).
2. The adsorption is reversible, as physisorption-based inhibitors can desorb under different conditions, such as temperature changes or dilution.
3. No significant interactions between MNATT molecules, meaning each adsorption site behaves independently.

As temperature increases, a slight enhancement in inhibition efficiency is observed, indicating that the adsorption remains effective but is not significantly strengthened by increasing thermal energy. This is consistent with physisorption, which is generally less sensitive to temperature changes than chemisorption. Higher MNATT concentrations lead to increased surface coverage, further validating the Langmuir isotherm assumption of monolayer adsorption**.** Beyond a concentration of 0.5 mM, the inhibition efficiency plateaus (~90.4%), suggesting that adsorption sites are saturated, preventing further

increases in protection. The HOMO energy level (-8.084 eV) indicates that MNATT can donate electrons, but the moderate energy prevents strong chemisorption. The LUMO energy (-4.552 eV) and small HOMO-LUMO gap (3.532 eV) suggest that charge transfer interactions occur but are not strong enough to form chemical bonds. The positive fraction of electron transfer ($\Delta N = 0.556$) suggests that some charge transfer takes place, reinforcing physical adsorption through electrostatic interactions rather than chemisorption.

Figure 10. Schematic Representation of the Physisorption-Based Corrosion Inhibition Mechanism of MNATT on Mild Steel in 1 M HCl.

3.8. Comparison of inhibition efficiency with similar inhibitors

The IE of MNATT in corrosive solution for mild steel in HCl has been evaluated and compared with other triazole derivatives reported in the literature. Desai and Indorwala, studied benzotriazole and demonstrated that the inhibition efficiencies of 93.46%,

70.16%, and 50.65% at a concentration of 25 mM in 1.0 M, 2.0 M, and 3.0 M HCl solutions, respectively. At a constant acid concentration of 1.0 M HCl, the IE increased with inhibitor concentration, reaching 93.46% at 25 mM [39]. Researchers investigated a triazole derivative namely 5-mercapto-1,2,4-triazole (EMTP) as anti-corrosion compound for steel in 1.0 M HCl, and found that the highest IE was 97% at 303 K. IE increased with rising concentration of tested inhibitor and decreased with increasing temperature [40]. Nahlé et al. synthesized two novel triazole derivatives, ethyl 2-(4-phenyl-1H-1,2,3-triazol-1-yl)acetate and 2-(4-phenyl-1H-1,2,3-triazol-1-yl)acetohydrazide, and evaluated ant-corrosion characteristics for steel in 1.0 M HCl and found that they significantly reduced the corrosion of mild steel with an inhibition rate close to that acquirable with other triazole-based inhibitors [41]. On the other hand, at an optimum concentration, MNATT reached 88.6% inhibition capacity in 5-hour-long immersion in 1 M HCl at 303 K. Whereas this is slightly less than some known effective inhibitors, it is quite notable that these high proportions of inhibition for MNATT come with low doses, a testimony to effectiveness as a corrosion inhibitor [42,43]. In summary, MNATT demonstrates inhibitive performance comparable to that of its triazole counterparts, with the added advantage of achieving this efficiency at significantly lower concentrations. Thus, this work first suggests that MNATT deserves being explored for consideration as a competent anticorrosive agent for metals in corrosive solutions.

While some corrosion inhibitors have shown higher inhibition efficiencies, MNATT offers several distinct advantages that make it a promising candidate for practical applications:

1. **High Efficiency at Low Concentration:** MNATT achieves 88.6% inhibition efficiency at just 0.5 mM, whereas many conventional inhibitors require higher concentrations (>10 mM) to reach comparable efficiency. This reduces the required inhibitor dosage, making MNATT more cost-effective in industrial applications [44,45].
2. **Physisorption-Based Protection at Room Temperature:** The adsorption of MNATT follows the Langmuir isotherm, and the free energy of adsorption ($\Delta G°_{ads}$ = -14.33 kJ·mol^{-1}) confirms a physisorption-driven mechanism. Unlike chemisorption-based inhibitors, which can lead to permanent modifications on metal surfaces, MNATT offers reversible adsorption, preventing potential long-term degradation or surface alteration [46,47].
3. **Potential for Industrial Application and Environmental Friendliness:** Many corrosion inhibitors involve complex synthesis routes or hazardous compounds, limiting their industrial scalability. MNATT is a structurally simple triazole derivative that exhibits high inhibition efficiency without the need for extensive modifications. Since MNATT primarily functions via physisorption, it can be easily removed or reapplied, making it suitable for dynamic environments such as oil pipelines, acid pickling processes, and chemical plants [48].
4. **Balanced Inhibitor Performance Across Various Conditions:** MNATT maintains stable inhibition efficiency over extended immersion times, as observed in weight loss experiments. Unlike some inhibitors that lose efficiency at higher temperatures, MNATT retains its protective capabilities with only a slight variation in efficiency [49].

5. **Theoretical and Experimental Validation:** This study integrates both experimental (weight loss tests, Langmuir adsorption studies) and theoretical (DFT calculations) analyses to understand MNATT's inhibition mechanism. The small HOMO-LUMO energy gap (3.532 eV) confirms high reactivity, enhancing electrostatic interactions with the mild steel surface, validating its adsorption and inhibition properties [50].

Although MNATT may exhibit slightly lower inhibition efficiency than some reported inhibitors, its ability to provide strong corrosion protection at lower concentrations, its physisorption-based mechanism, and its cost-effectiveness make it a highly viable inhibitor for industrial applications. Further optimization and combination with synergistic additives could enhance its effectiveness and broaden its scope of use in corrosion control strategies.

4. Conclusion

The present investigation studied the anti-pitting activity of MNATT toward mild steel in 1 M HCl by employing weight loss techniques, Langmuir model, and DFT. The key findings of the research are summarized as follows:

1. Corrosion Inhibition Performance: IE of MNATT increased with concentration, reaching a maximum of 88.6% at 0.5 mM after 5 hours of immersion at 303 K. The temperature-dependent studies (303-333 K) showed a slight increase in inhibition efficiency, suggesting that adsorption remains effective at elevated temperatures.

2. Adsorption Mechanism: The adsorption behavior followed the Langmuir isotherm, indicating the formation of a monolayer on the steel surface. The calculated free energy (ΔG_{ads}^{o} = -14.33 $KJmol^{-1}$) confirmed that the inhibition process is spontaneous and dominated by physisorption. The physisorption mechanism is attributed to electrostatic interactions between MNATT molecules and the positively charged mild steel surface.
3. Quantum Chemical Insights: The HOMO (-8.084 eV) and LUMO (-4.552 eV) energy levels indicate the molecule's capability to donate and accept electrons, facilitating interaction with the metal surface. The small HOMO-LUMO energy gap (3.532 eV) confirms high molecular reactivity, enhancing MNATT's adsorption and inhibition efficiency. The fraction of electron transfer (ΔN = 0.556) further supports the electron donation from MNATT to Fe, stabilizing the inhibitor-metal interaction.
4. Comparison with Similar Inhibitors: MNATT exhibited comparable IE to other triazole derivatives, despite being effective at significantly lower concentrations. Unlike some inhibitors that require high concentrations (>10 mM), MNATT achieved high IE (~90%) at just 0.5 mM, making it an economically viable option.

In addition to its scientific significance, the findings of this study offer important industrial and environmental implications. Due to its high inhibition efficiency at low concentrations, MNATT demonstrates strong potential for use in various acidic industrial environments, including oil well acidizing, acid pickling, and pipeline protection. By reducing the required dosage of inhibitor, MNATT may help minimize chemical

consumption, thus lowering operational costs and environmental impact. Furthermore, its mechanism of physisorption-based protection supports its potential for use in sustainable corrosion management strategies, making it a promising candidate for safer and more efficient industrial corrosion control systems.

5. References

1. Vaszilcsin N, Ordodi V, Borza A. Corrosion inhibitors from expired drugs. Inter J Pharm. 2012; 431(1-2):241- 4. https://doi.org/10.1016/j.ijpharm. 2012. 04.015.
2. Jalab R, Saad MA, Sliem MH, Abdullah AM, Hussein IA. An eco-friendly quaternary ammonium salt as a corrosion inhibitor for carbon steel in 5 M HCl solution: theoretical and experimental investigation. Molecules. 2022; 27(19):6414. https:// doi.org/10.3390/molecules27196414
3. Al-Shafey HI, Hameed RA, Ali FA, Aboul-Magd AE, Salah M. Effect of expired drugs as corrosion inhibitors for carbon steel in 1M HCL solution. Int J Pharm Sci Rev Res. 2014; 27(1):146-52. https://doi. org/10.15344/2394-8376/2024/146.
4. Dehghani A, Ghahremani P, Mostafatabar AH, Ramezanzadeh B. Plant extracts: Probable alternatives for traditional inhibitors for controlling alloys corrosion against acidic media-A review. Biomass Con Bioref. 2024; 14(6):7467-86. https://doi.org/10. 1007/s13399-023-03907-0.
5. Dehghani A, Berdimurodov E, Verma C, Verma DK, Berdimuradov K, Quraishi MA, Aliev N. Constructing efficacy: A novel perspective on organic corrosion inhibitors and interfacial interactions. Chem Papers. 2024; 78(3):1367-97. https://doi.org/10.1007/s11696- 023-02586-4.

6. Zunita M, Rahmi VA. Advancement of plant extract/ionic liquid-based green corrosion inhibitor. Chem Africa. 2024; 7(2):505-38. https://doi.org/10. 1007/s42250-023-00426-0.

7. Akpan ED, Singh AK, Lgaz H, Quadri TW, Shukla SK, Mangla B, Dwivedi A, Dagdag O, Inyang EE, Ebenso EE. Coordination compounds as corrosion inhibitors of metals: A review. Coord Chem Rev. 2024; 499:215503. https://doi.org/10.1016/j.ccr. 2024. 215503.

8. Mortadi K, El Amri A, Ouakki M, Hsissou R, Jebli A, Lebkiri A, Safi Z, Wazzan N, Berisha A, Cherkaoui M, Hbaiz EM. Electrochemical and theoretical studies on a bioactive Juniperus oxycedrus essential oil as a potential and ecofriendly corrosion inhibitor for mild steel in 1.0 M HCl environment. Inorg Chem Commun. 2024; 112196. https://doi.org/ 10.1016/j.inoche.2024.112196.

9. Lavanya M, Ghosal J, Rao P. A comprehensive review of corrosion inhibition of aluminium alloys by green inhibitors. Canadian Metallur Quart. 2024; 63(1):119-29. https://doi.org/10.1080/00084433.2024. 1132326.

10. Sehrawat R, Vashishth P, Bairagi H, Shukla SK, Kumar H, Ji G, Mangla B. Coordination bonding and corrosion inhibition characteristics of chalcone compounds for metals: An inclusive review based on experimental as well as theoretical perspectives. Coordin Chem Rev. 2024; 514:215820. https://doi. org/10.1016/j.ccr.2024.215820.

11. AL Salihi HA, Mahdi RR, Al-Amiery A, Al-Azzawi WK, Kadhum AA. Exploring the efficacy of polysaccharides as green corrosion inhibitors: A comprehensive review. Starch-Stärke. 2024; 2300234. https://doi.org/10.1002/star.202300234

12. Berrissoul A, Exploitation of a new green inhibitor against mild steel corrosion in HCl: Experimental, DFT and MD simulation approach. J Mol Liq. 2022; 349: 118102.
13. Ouakki M, Galai M, Cherkaoui M. Imidazole derivatives as efficient and potential class of corrosion inhibitors for metals and alloys in aqueous electrolytes: A review. J Mol Liq. 2022: 345: 117815.
14. Sun X, Qiang Y, Hou B, Zhu H, Tian H. Cabbage extract as an eco-friendly corrosion inhibitor for X70 steel in hydrochloric acid medium. J Mol Liq. 2022; 362: 119733.
15. Ghaderi M, Saadatabadi A, Mahdavian M, Haddadi A. pH-sensitive polydopamine–La (III) complex decorated on carbon nanofiber toward on-demand release functioning of epoxy anti-corrosion coating. Langmuir. 2022; 38: 11707-11723.
16. Agus K, Ridhova A, Priyotomo G, Elya B, Maksum A, Sadeli Y, utopo S, Aditiyawarman S, Riastuti R, Soedarsono J. Development of white tea extract as green corrosion inhibitor in mild steel under 1 M hydrochloric acid solution. Eastern-European J Enterprise Technol. 2021; 12: 110. https://doi.org/10.15587/1729-4061.2021.224435
17. Emmanuel JK. Corrosion protection of mild steel in corrosive media, a shift from synthetic to natural corrosion inhibitors: a review. Bulletin Nation Res Cent. 2024; 48(1):26. https://doi.org/10.1186/s42269- 023-00219-3.
18. ASTM International, Standard Practice for Preparing, Cleaning, and Evaluating Corrosion Test, 2011, 1-9.

19. NACE International, Laboratory Corrosion Testing of Metals in Static Chemical Cleaning Solutions at Temperatures below 93 °C (200 °F), TM0193-2016- SG, 2000

20. M.J. Frisch, G.W. Trucks, H.B. Schlegel, G.E. Scuseria, M.A. Robb, J.R. Cheeseman, J.A. Montgomery, Jr., T. Vreven, K.N. Kudin, J.C. Burant, J.M. Millam, S.S. Iyengar, J. Tomasi, V. Barone, B. Mennucci, M. Cossi, G. Scalmani, N. Rega, G.A. Petersson, H. Nakatsuji, M. Hada, M. Ehara, K. Toyota, R. Fukuda, J. Hasegawa, M. Ishida, T. Nakajima, Y. Honda, O. Kitao, H. Nakai, M. Klene, X. Li, J.E. Knox, H.P. Hratchian, J.B. Cross, V. Bakken, C. Adamo, J. Jaramillo, R. Gomperts, R.E. Stratmann, O. Yazyev, A.J. Austin, R. Cammi, C. Pomelli, J.W. Ochterski, P.Y. Ayala, K. Morokuma, G.A. Voth, P. Salvador, J.J. Dannenberg, V.G. Zakrzewski, S. Dapprich, A.D. Daniels, M.C. Strain, O. Farkas, D.K. Malick, A.D. Rabuck, K. Raghavachari, J.B. Foresman, J.V. Ortiz, Q. Cui, A.G. Baboul, S. Clifford, J. Cioslowski, B.B. Stefanov, G. Liu, A. Liashenko, P. Piskorz, I. Komaromi, R.L. Martin, D.J. Fox, T. Keith, M.A. AlLaham, C.Y. Peng, A. Nanayakkara, M. Challacombe, P.M.W. Gill, B. Johnson, W. Chen, M.W. Wong, C. Gonzalez and J.A. Pople, Gaussian 03, Revision B.05, Gaussian, Inc., Wallingford CT, 2004.

21. Zhao Y, Teng X, Xu Z. The scale inhibition mechanism of sodium humate on heat transfer surface: Insights from electrochemical experiments, quantum chemical calculations, and molecular dynamics simulation. Inter J Heat Mass Transfer. 2024; 220:124966. https://doi.org/10.1016/j.ijheatmasstransfer. 2023.124966.

22. Koopmans T. Über die Zuordnung von Wellenfunktionen und Eigenwerten zu den einzelnen Elektronen eines Atoms. Physica. 1934; 1(1-6):104-13. https://doi.org/10.1016/S0031-8914(34)90011-2.

23. Namdar-Asl H, Fakheri F, Pour-Ali S, Tavangar R, Hejazi S. Synthesis and corrosion inhibition study of 1-aminobenzotriazole for mild steel in HCl solution: electrochemical, surface analysis, and theoretical investigations. Prog Color Colorant Coat. 2024; 17(1): 61-74. https://doi.org/10.30502/PCCC.2023.359903. 1015.

24. Touir R, Errahmany N, Rbaa M, Benhiba F, Doubi M, Kafssaoui EE, Lakhrissi B. Experimental and computational chemistry investigation of the molecular structures of new synthetic quinazolinone derivatives as acid corrosion inhibitors for mild steel. J Mol Struct. 2024; 1303:137499. https://doi.org/10. 1016/ j.molstruc.2023.137499.

25. Coy-Barrera CA, Quiroga D. In silico evaluation for the design of coumarin-type compounds based on phenol and naphthol rings as a coating in carbon steel corrosion processes: DFT B3LYP calculations, synthesis and electrochemical characterization. Prog Org Coat. 2024; 188:108266. https://doi.org/10.1016/ j. porgcoat.2023.108266.

26. Sheit HM, Mohan KS, Gunavathy KV, Mohamed MV, Subhapriya P, Samsathbegum A, Sindhuja GH. Investigation on the corrosion inhibition efficiency of 2,4-diphenyl-3-aza bicyclo [3.3.1] nonan-9-one in carbon steel immersed in acidic media. Chem Phys Impact. 2024; 8:100521. https://doi.org/10.1016/j. chphi. 2023.100521.

27. Anadebe VC, Chukwuike VI, Nayak KC, Ebenso EE, Barik RC. Combined electrochemical, atomic scaleDFT and MD simulation of Nickel based metal organic framework (Ni-MOF) as corrosion inhibitor for X65 pipeline steel in CO_2-saturated

brine. Mater Chem Phys. 2024; 312:128606. https://doi.org/10. 1016/j.matchemphys.2023.128606.

28. Laarioui A, Chaouki I, Hmada A, El Magri A, Errahmany N, El Hajri F, Dkhireche N, Bakkali S, Touir R, Boukhris S. Corrosion inhibition effect of the synthetized chromen-6-one derivatives on mild steel in 1.0 M HCl electrolyte: electrochemical, spectroscopic and theoretical studies. Mor J Chem. 2024; 12(2):570-93. https://doi.org/10.48317/IMIST. PRSM/morjchem-v12i2.40860.
29. Pai GD, Rathod MR, Rajappa SK, Kittur AA. Effect of tabebuia heterophylla plant leaves extract on corrosion protection of low carbon steel in 1M HCl medium: Electrochemical, quantum chemical and surface characterization studies. Results Surf Inter. 2024; 15:100203. https://doi.org/10.1016/j.rsurfin. 2023. 100203.
30. Dahmani K, Galai M, Rbaa M, Ech-Chebab A, Errahmany N, Guo L, AlObaid AA, Hmada A, Warad I, Touhami ME, Cherkaoui M. Evaluating the efficacy of synthesized quinoline derivatives as corrosion inhibitors for mild steel in acidic environments: An analysis using electrochemical, computational, and surface techniques. J Mol Struct. 2024; 1295:136514. https://doi.org/10.1016/j.molstruc.2023.136514.
31. Akrom M, Rustad S, Dipojono HK. A machine learning approach to predict the efficiency of corrosion inhibition by natural product-based organic inhibitors. Phys Scripta. 2024; 99(3):036006. https://doi.org/10.1088/1402-4896/ace0d2.
32. Fernandes CM, Coutinho MS, Leite MC, Martins V, Batista MP, Faro LV, Al-Rashdi AA, Silva JC, Batalha PN, Lgaz H, Ponzio EA. Green-synthetized βamino-α-carbethoxy ethyl acrylates as corrosion inhibitors for mild steel in acid media:

Experimental performance evaluation and atomic/molecular-level modeling. Inorg Chem Commun. 2024; 159:111722. https://doi.org/10.1016/j.inoche.2023.111722.

33. Essien KE, Okon EJ, Archibong IN, Okon OE, George IE. Experimental, Quantum chemical and IR spectroscopy studies on the corrosion inhibition of mild steel by 3,5-dimethyl-4-nitroisoxazole in HCl solutions. J Mater Environ Sci. 2024; 15(1):136. https://doi.org/10.26872/jmes.2021.12.6.40.
34. Quy Huong D, Duong T, Nam PC. Effect of the structure and temperature on corrosion inhibition of thiourea derivatives in 1.0 M HCl solution. ACS omega. 2019 Aug 26;4(11):14478-89. https://doi.org/10.1021/acsomega.9b01599
35. Dehghani A, Berdimurodov E, Verma C, Verma DK, Berdimuradov K, Quraishi MA, Aliev N. Constructing efficacy: A novel perspective on organic corrosion inhibitors and interfacial interactions. Chem Papers. 2024; 78(3):1367-97. https://doi.org/10.1007/s11696- 023-02523-0.
36. Wang Q, Zhou X, Zhao C, Wang R, Sun Y, Yan Z, Li X. Corrosion inhibition behavior and theoretical study on carbon steel in H_2SO_4 by Schizochytrium extract. Chem Papers. 2024; 78(2):909-26. https://doi.org/ 10.1007/s11696-023-02524-z.
37. Mamand DM, Kak Anwer TM, Qadr HM. Corrosion inhibition performance of organic compounds and theoretical calculations based on density functional theory (DFT). Corr Rev. 2024; 42(1):1-5. https://doi. org/ 10.1515/corrrev-2023-0015.
38. Crisan M, Muntean C, Chumakov Y, Plesu N. Investigating the corrosion inhibition mechanisms of alkanolammonium salts: a case study with ethylethanolammonium 4-nitrobenzoate on carbon steel in saline solution. Appl Sci. 2024; 14(5):1832. https://doi.org/ 10.3390/app14051832.

39. Pourmohseni M, Rashidi A, Karimkhani M. Preparation of corrosion inhibitor from natural plant for mild steel immersed in an acidic environment: experimental and theoretical study. Sci Reports. 2024;14(1):7937. https://doi.org/10.1038/s41598-023-34440-3.

40. Al-Amiery A, Shaker LM, Kadhum AA, Takriff MS. Synthesis, characterization and gravimetric studies of novel triazole-based compound. Inter J Low-Carbon Technol. 2020; 15(2):164-70. https://doi.org/10.1093/ ijlct/ctz067.

41. Nahlé A, Salim R, El Hajjaji F, Aouad MR, Messali M, Ech-Chihbi E, Hammouti B, Taleb M. Novel triazole derivatives as ecological corrosion inhibitors for mild steel in 1.0 M HCl: experimental & theoretical approach. RSC advances. 2021;11(7):4147-62. https://doi.org/10.1039/D0RA09679B

42. . Elabbasy HM, Toghan A, Gadow HS. Cysteine as an eco-friendly anticorrosion inhibitor for mild steel in various acidic solutions: electrochemical, adsorption, surface analysis, and quantum chemical calculations. ACS Omega. 2024; 9(11):13391-411. https://doi.org/ 10.1021/acsomega.3c06066.

43. Toghan A, Farag AA, Alduaij OK, Elabbasy HM, Dardeer HM, Masoud EM, Fawzy A, Gadow HS. Electrochemical, gravimetric, quantum chemical and computational investigations on an effective synthetic chlorinated cyclic imide derivative as a corrosion inhibitor for carbon steel in sulfuric acid solution. J Mol Struct. 2024; 1307:138040. https://doi.org/10. 1016/ j.molstruc.2023.138040.

44. Verma C, Dubey S, Bose R, Alfantazi A, Ebenso EE, Rhee KY. Zwitterions and betaines as highly soluble materials for sustainable corrosion protection: Interfacial

chemistry and bonding with metal surfaces. Adv Coll Interf Sci. 2024:103091. https://doi.org/10. 1016/j.cis.2023.103091.

45. Verma C, Al-Moubaraki AH, Alfantazi A, Rhee KY. Heterocyclic amino acids-based green and sustainable corrosion inhibitors: Adsorption, bonding and corrosion control. J Clean Prod. 2024:141186. https://doi.org/10.1016/j.jclepro.2023.141186.
46. Liu Y, Shi J. Recent progress and challenges of using smart corrosion inhibitors in reinforced concrete structures. Const Building Mater. 2024; 411:134595. https://doi.org/10.1016/j.conbuildmat.2023.134595.
47. Song S, Yan H, Cai M, Huang Y, Fan X, Zhu M. Constructing mechanochemical durable superhydrophobic composite coating towards superior anticorrosion. Adv Mater Technol. 2022; 7(6):2101223. https://doi.org/10.1002/admt.202101223.
48. Pistone A, Scolaro C, Visco A. Mechanical properties of protective coatings against marine fouling: A review. Polymers. 2021; 13(2):173. https://doi.org/10.3390/polym13020173.
49. Jamali SS, Wu Y, Homborg AM, Lemay SG, Gooding JJ. Interpretation of stochastic electrochemical data. Current Opinion Electrochem. 2024; 46:101505. https://doi.org/10.1016/j.coelec. 2023. 101505.
50. Shetty S, Rao P, Kedimar N, Rao SA. Electrochemical and quantum chemical investigation to evaluate corrosion inhibition performance of therapeutic drug. Canadian Metal Quarterly. 2024; 63(2):468-82. https://doi.org/10.1007/s42641-023-00280-8